The American Journal of Pathology, Vol. 184, No. 6, June 2014

The American Journal of
PATHOLOGY
ajp.amjpathol.org

SHORT COMMUNICATION

Loss of Corneal Sensory Nerve Fibers in SIV-Infected Macaques

An Alternate Approach to Investigate HIV-Induced PNS Damage

Jamie L. Dorsey,* Lisa M. Mangus,*† Jonathan D. Oakley,‡ Sarah E. Beck,*† Kathleen M. Kelly,*† Suzanne E. Queen,* Kelly A. Metcalf Pate,* Robert J. Adams,* Carl F. Marfurt,§ and Joseph L. Mankowski*†¶

From the Departments of Molecular and Comparative Pathobiology, Pathology,† and Neurology,¶ Johns Hopkins University School of Medicine, Baltimore, Maryland; Voxeleron,‡ Pleasanton, California; and the Department of Anatomy and Cell Biology,§ Indiana University School of Medicine-Northwest, Gary, Indiana*

Accepted for publication February 11, 2014.

Address correspondence to Joseph L. Mankowski, D.V.M., Ph.D., Department of Molecular and Comparative Pathobiology, Johns Hopkins University, 733 N. Broadway, BRB 827, Baltimore, MD 21205-2196. E-mail: jmankows@jhmi.edu.

Peripheral neuropathy is the most frequent neurological complication of HIV infection, affecting more than one-third of infected patients, including patients treated with antiretroviral therapy. Although emerging noninvasive techniques for corneal nerve assessments are increasingly being used to diagnose and monitor peripheral neuropathies, corneal nerve alterations have not been characterized in HIV. Here, to determine whether SIV infection leads to corneal nerve fiber loss, we immunostained corneas for the nerve fiber marker βIII tubulin. We developed and applied both manual and automated methods to measure nerves in the corneal subbasal plexus. These counting methods independently indicated significantly lower subbasal corneal nerve fiber density among SIV-infected animals that rapidly progressed to AIDS compared with slow progressors. Concomitant with decreased corneal nerve fiber density, rapid progressors had increased levels of SIV RNA and CD68-positive macrophages and expression of glial fibrillary acidic protein by glial satellite cells in the trigeminal ganglia, the location of the neuronal cell bodies of corneal sensory nerve fibers. In addition, corneal nerve fiber density was directly correlated with epidermal nerve fiber length. These findings indicate that corneal nerve assessment has great potential to diagnose and monitor HIV-induced peripheral neuropathy and to set the stage for introducing noninvasive techniques to measure corneal nerve fiber density in HIV clinical settings. *(Am J Pathol 2014, 184: 1652–1659; http://dx.doi.org/10.1016/j.ajpath.2014.02.009)*

Peripheral neuropathy (PN) is the most frequent neurological complication caused by HIV-1, affecting more than one-third of infected persons, including patients receiving combination antiretroviral therapy.[1,2] The typical clinical presentation is known as distal sensory polyneuropathy, a length-dependent neuropathy that is characterized by bilateral aching, painful numbness or burning, and is most pronounced in the lower extremities.[3,4] Although HIV-induced PN (HIV-PN) is not life threatening, this debilitating disorder greatly compromises patient quality of life.[1] Currently, skin biopsy is the accepted standard for measuring the loss of small, unmyelinated C fibers in the epidermis, one of the earliest detectable signs of damage to the peripheral nervous system (PNS).[5–7] However, skin biopsy is an invasive procedure, and longitudinal assessment requires repeated surgical biopsies. Electrophysiological testing to measure properties of peripheral nerve conduction is not considered a viable alternative because

Supported by NIH grants NS055651, MH070306, NS077869, T32 OD011089, and P40 OD013117 (J.L.M.).
Disclosures: None declared.

http://dx.doi.org/10.1016/j.ajpath.2014.02.009

current methods lack the sensitivity required to detect damage to small, unmyelinated fibers, especially in early stages of disease.[8,9] For these reasons, new, sensitive, noninvasive methods of assessing small fiber nerve damage are urgently needed to detect and monitor PN in persons infected with HIV.

Like HIV, small sensory nerve fiber loss is common in patients with diabetes mellitus and results in a clinical syndrome that closely resembles HIV distal sensory polyneuropathy.[10] Of interest, studies have documented the utility of measuring changes in corneal sensory innervation to track diabetic neuropathy as an alternative to measuring epidermal nerve fiber (ENF) density via skin biopsy. In particular, decreases in the nerve density in the corneal subbasal plexus (SBP) have been reported in both isolated corneal whole mount studies and by noninvasive *in vivo* corneal confocal microscopy (CCM).[11–15]

Although corneal nerve assessments have found increasing value as a surrogate to evaluate ENFs in diabetic PN, the use of corneal alterations in tracking HIV-induced neuropathy has yet to be explored. To study the pathogenesis of HIV-induced PNS disease, our group developed a SIV-infected macaque model that closely recapitulates key PNS alterations seen in patients with HIV with PN. These changes include macrophage infiltration, SIV replication, and neuronal loss in sensory ganglia, including the trigeminal ganglia, which house the cell bodies of sensory neurons that innervate the cornea.[16,17] In this report, we aimed to determine whether SIV infection leads to decreases in corneal nerve fiber (CNF) density, whether changes in corneal nerves correspond with the extent of SIV replication and the severity of cellular immune responses in the trigeminal ganglia, and whether CNF density correlates with ENF length, thereby setting the stage for follow-up CCM investigation. To achieve optimal immunostaining of the corneal SBP, we modified an immunohistochemical staining method developed by Marfurt et al.[18] Because conventional image analysis of the corneal nerve is labor intensive and requires trained observers, we developed two novel counting methods: a relatively simple manual counting method of nerve fibers and an automated method of nerve detection and counting to facilitate efficient, objective assessment of nerve fiber density.

Materials and Methods

Animals

Male juvenile pigtailed macaques (*Macaca nemestrina*) were inoculated intravenously with either a combination of the infectious clone SIV/17E-Fr and the viral swarm SIV/DeltaB670 ($n = 7$) or with the infectious clone SIV/17E-Fr ($n = 4$).[19] Serology was negative for SIV, simian T-cell leukemia virus, and simian type D retrovirus for all macaques before inoculation. For control purposes, corneas also were obtained from three additional uninfected macaques. Animals were housed in Johns Hopkins University facilities that are fully accredited by the Association for Assessment and Accreditation of Laboratory Animal Care International. Macaques were fed a commercial macaque diet (Harlan, Indianapolis, IN), given water *ad libitum*, and provided with environmental enrichment daily. All procedures were approved by the Johns Hopkins University Institutional Animal Care and Use Committee and were conducted in accordance with guidelines set forth in the Animal Welfare Regulations (US Department of Agriculture) and the Guide for the Care and Use of Laboratory Animals (Office of Laboratory Animal Welfare).

Viral Load

To evaluate SIV RNA levels, RNA was extracted from frozen trigeminal ganglia or plasma. Viral load was measured by quantitative RT-PCR with the use of primers to quantitate SIV gag.[20]

Cornea IHC

After euthanasia, an 8-mm biopsy punch was used to remove the central cornea from the eye. Corneas were immediately placed in 0.1 mol/L PBS and stored at 4°C for 8 hours before preservation in 10% neutral-buffered formalin. Corneas were then fixed overnight at 4°C, rinsed three times in PBS, and cryoprotected overnight at 4°C in 20% glycerol/0.1 mol/L Sørensen's phosphate buffer. Before immunostaining, a 5-mm biopsy punch was used to remove the central corneal button, which was then immunostained as a free-floating whole mount. To enhance permeability, whole mounts were incubated for 48 hours at 37°C in 0.01% hyaluronidase (type IV-S; Sigma-Aldrich, St. Louis, MO) and 0.1% EDTA (Sigma-Aldrich) in 0.1 mol/L PBS (pH 5.3). Corneal buttons were then washed three times for 15 minutes each in PBS that contained 0.3% Triton X-100 and also between each subsequent immunostaining step. Nonspecific labeling was blocked by incubation at room temperature for 2 hours in blocking serum (1% bovine serum albumin in PBS that contained 0.3% Triton X-100) before a 4-day incubation at room temperature with a mouse monoclonal antibody against the neuronal marker βIII tubulin (1:500; Promega Corporation, Madison, WI). Corneal buttons were then incubated in secondary antibody (biotinylated goat anti-mouse IgG, 1:200; Vector Laboratories, Burlingame, CA) followed by avidin-biotin-horseradish peroxidase complex (Vectastain Elite ABC Reagent; Vector Laboratories) for 2 hours each at room temperature and subsequent detection with the diaminobenzidine chromogen (Sigma-Aldrich) after incubation for 10 to 15 minutes. After washing, corneas were mounted on chrome alum-gelatin–coated slides and air-dried overnight. Tissue slides were then washed in distilled water, dehydrated in graded alcohols, cleared in HistoClear (National Diagnostics, Atlanta, GA), and coverslipped with Permount (Fisher Scientific, Pittsburgh, PA).

Quantitative Assessment of SBP: Image Acquisition

For each cornea, images of five ×200 fields (one field from each quadrant and one field from the central cornea) of the SBP were captured with a Retiga 2000R digital camera (QImaging, Surrey, BC, Canada) mounted on a Nikon E600 microscope (Nikon, Tokyo, Japan). Several serial Z-stack images were taken of each field to accommodate for the curvature of the cornea, thus bringing the entire SBP of the field into a single focused plane. The subregions of SBP in focus for each image were selected in Adobe Photoshop CS4 software version 11.0 (Adobe Systems, San Jose, CA) and autoblended to assemble a single cohesive image of the subbasal nerve plexus for each field. The blended images were subsequently used in the quantitative assessment of nerve fiber density.

Manual Assessment

Corneal SBP nerves were counted with Stereo Investigator software version 9 (MicroBrightField Inc, Colchester, VT) to draw three transect lines across each image oriented perpendicular to the longitudinal subbasal nerve fibers. The number of nerves crossing each transect was counted and then divided by the total transect length. For each image, the number of nerves crossing each of the three transects was averaged, and the final mean number of corneal nerves per millimeter was derived from the five images for each animal.

Automated Assessment

To automate nerve counts in the cornea, a custom algorithm was developed specifically to quantify nerve fibers in SBP images to emulate the manual counting method. First, anisotropic diffusion filtering was applied to reduce noise while preserving the structure of each image.[21] The linear structure of the nerves was then enhanced across various scales with the use of Frangi's Hessian-based filter.[22] To exploit the piecewise linearity of the nerves, the image was subdivided into smaller regions in which nerves exhibited the same orientation. Next, the subimages were reoriented to find the best (ie, most prominent) orientation of the nerves, defined as minimal entropy of the distribution of image data in the resulting 1D profile. The number of visible nerves was determined by summing image data along the most prominent orientation and then counting the peaks in the 1D profile, with each peak representing a single nerve fiber. The nerve count was derived cumulatively from the sum of the peaks per image for each of the five images.

Trigeminal Ganglia IHC

IHC was performed on HistoChoice-fixed (HistoChoice Tissue Fixative; Amresco, Solon, OH) paraffin-embedded sections of trigeminal ganglia. Tissue sections were deparaffinized by heating for 30 minutes at 60°C, cleared in changes of HistoClear (National Diagnostics), and then rehydrated in a graded series of alcohol. Slides were pretreated for antigen retrieval by heating with 0.01 mol/L sodium citrate (pH 6.0) before immunostaining. Endogenous peroxidases were blocked with 3% hydrogen peroxide in methanol, then nonspecific labeling was blocked with dilute block (Vector Laboratories). Sections were incubated in the appropriate primary antibody dilution [CD68, 1:4000, clone KP1, and glial fibrillary acidic protein (GFAP), 1:80,000; Dako, Carpinteria, CA] for 1 hour, followed by biotinylated anti-mouse/rabbit secondary antibody and avidin-biotin-horseradish peroxidase complex (Vectastain Elite ABC Reagent; Vector Laboratories) for 30 minutes each with subsequent detection with the diaminobenzidine chromogen (Vector Laboratories). Tissue sections were then washed, cleared, and coverslipped with Permount (Fisher Scientific). The amount of immunostaining for the macrophage marker CD68 and satellite cell marker GFAP was measured by digitized image analysis as described.[17] For each trigeminal ganglion, 20 nonoverlapping fields at ×200 magnification were captured with a Retiga 2000R digital camera (QImaging) mounted on a Nikon E600 microscope (Nikon). Binarized images were then analyzed with iVision imaging software version 4.0.14 (BioVision Technologies, Exton, PA). The mean total area occupied by the immunopositive pixels in the trigeminal ganglion was calculated for each animal.

ENF IHC

To measure ENF density in the skin of the plantar footpad surface of the hind limb, 3-mm diameter punch footpad samples were obtained at necropsy from the identical site. Footpad skin sections were fixed for 12 to 24 hours in 2% paraformaldehyde/lysine/periodate fixative at 4°C, rinsed with 0.08 mol/L Sørensen's phosphate buffer, and then transferred to cryoprotective buffer (20% glycerol in 0.08 mol/L Sørensen's phosphate buffer) until processed as previously described.[23] Cryoprotected samples were sectioned at a thickness of 50 μm on a sliding microtome and then immunostained for PGP9.5, a pan axonal marker (1:2000; Chemicon, Temecula, CA), as previously described.[24,25]

Measurement of ENF Length

PGP9.5 ENF length was quantified with unbiased stereology methodology by using the space ball probe on Stereo Investigator software version 9 (MBF Bioscience, Williston, VT) described by Ebenezer et al[26,27] and Mouton.[28] Three 50-μm PGP9.5 immunostained sections from one plantar footpad biopsy from each animal were measured. The area of interest was defined as the epidermal region that extended from the epidermal/dermal junction to the stratum corneum and was drawn under a Nikon 4×/0.2 Plan Apo objective on a Nikon Eclipse E600 light microscope. The ENF length was measured with a Nikon 60×/1.40 oil Plan Apo objective. The radius of the hemisphere probe was 30 μm with a

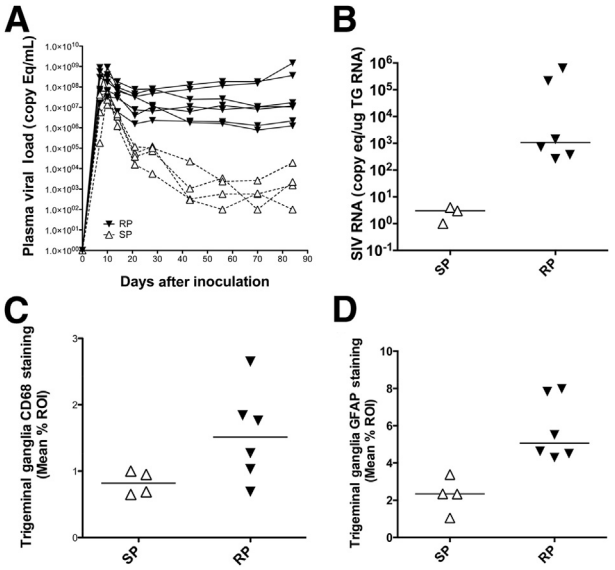

Figure 1 SIV PVL over time and SIV-induced alterations in SIV RNA, CD68, and GFAP expressions in trigeminal ganglia according to severity of SIV infection. **A:** Longitudinal plasma SIV RNA levels depict a markedly lower viral set point among the singly inoculated macaques, classified as SPs, than do the dual-inoculated macaques that sustained high plasma viremia and progressed to AIDS, classified as RPs. **B:** A scatter plot depicting the SIV viral load in the TG indicates increased SIV replication in the TG of RPs compared with SPs. **C:** CD68 immunostaining of the TG indicates a marked increase in macrophage activation and infiltration in the TG among the RPs, concomitant with the increased severity of SIV infection. **D:** GFAP immunostaining of glial satellite cells in the TG was similarly significantly increased among the RPs. **Horizontal lines** represent median values. $P = 0.024$ (**B**) and $P = 0.0095$ (**D**), both by Mann-Whitney test. ROI, region of interest; RP, rapid progressor; SP, slow progressor; TG, trigeminal ganglion.

guard zone of 2 μm. Only nerve fibers within the epidermis were counted. The results were expressed as the length of PGP9.5 nerve fibers. All stereology measurements were obtained with DAT files of Stereo Investigator.[27]

Results

SIV Disease Progression: Defining Rapid- versus Slow-Progressing SIV Groups

Seven animals were dual-inoculated with SIV/17E-Fr, an infectious clone, and with SIV/DeltaB670, an immunosuppressive swarm. An additional four animals were inoculated with only the molecular clone SIV/17E-Fr. To track SIV disease progression, plasma viral loads (PVLs) were measured by quantitative RT-PCR in longitudinal samples obtained from acute through terminal disease time points. During acute infection, all animals developed similar high PVLs with peak SIV RNA levels at 10 to 14 days after inoculation of 10^7 to 10^9 RNA copies/mL (Figure 1A). Among the dual-inoculated animals, the viral set point remained high, and at the time of sacrifice (84 days after inoculation), dual-inoculated animals had progressed to AIDS with severely diminished $CD4^+$ T-lymphocyte counts (median terminal PVL $= 1.18 \times 10^7$ copies/mL, median terminal $CD4^+$ T cells/μL $= 276$). In contrast, the singly inoculated animals had a much lower PVL set point after acute infection that continued to the time of sacrifice (median terminal PVL $= 1.89 \times 10^3$ copies/mL) and also maintained a significantly higher $CD4^+$ T-lymphocyte count (median terminal $CD4^+$ T cells/μL $= 989$; $P = 0.0061$) than did the dual-inoculated macaques. Given these differences between groups, dual-inoculated versus singly inoculated animals were classified as rapid progressors and slow progressors, respectively, in subsequent group comparisons.

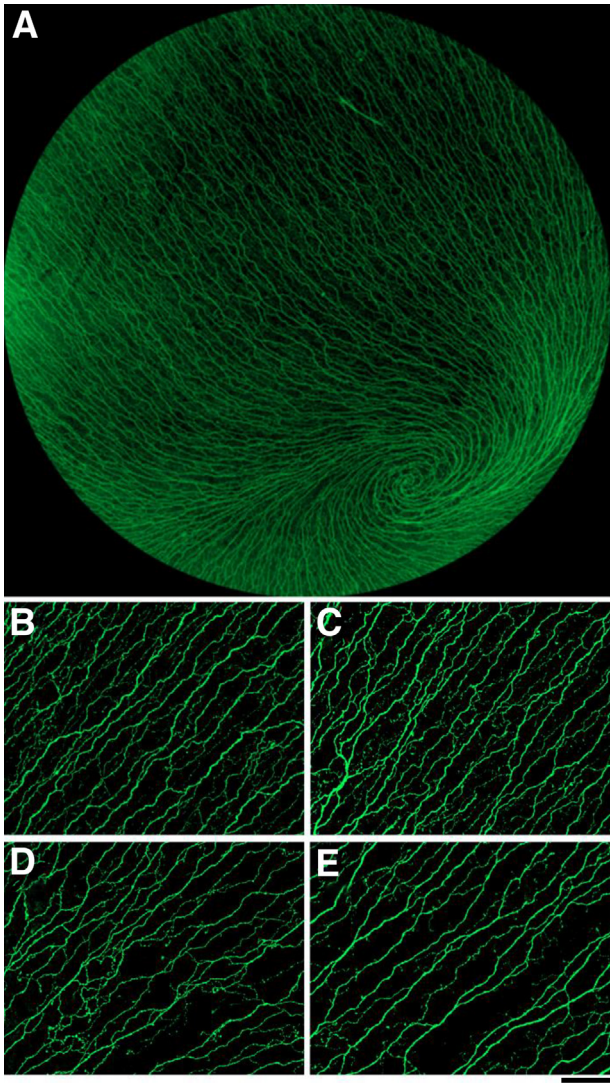

Figure 2 Representative βIII tubulin immunostaining of corneal SBP nerve fibers in rapid progressors compared with slow progressors. **A:** Image of the corneal SBP of 5 mm corneal whole mount immunostained for the neuronal marker βIII tubulin shows the dense sensory nerve fibers throughout the cornea. **B** and **C:** Representative images of the SBP among slow progressors show dense, regularly spaced nerve fibers. **D** and **E:** In contrast, images of the SBP from the rapid progressors exhibit lower CNF density than the slow progressors. For image comparison, black and white images were pseudocolored to green and black with the use of iVision software. Scale bar = 100 μmol/L. Original magnifications: ×20 (**A**); ×200 (**B**–**E**).

CNF Density

To determine whether SIV infection induced nerve fiber loss in the corneal SBP, cornea whole mounts 5 mm in diameter were immunostained for the neuronal marker βIII tubulin (Figure 2A). Visual inspection of these images indicated lower nerve fiber density in the rapid progressor group than in the slow progressor group (Figure 2, B–E). To measure the number of CNFs, identical ×200 images of the SBP were analyzed both by counting manually and by an automated counting method (Figure 3, A–D). Manual and automated CNF counts showed a strong, positive correlation between nerve fiber counts ($P = 0.0004$, $r = 0.90$), indicating excellent agreement between the two counting methods (Figure 3E). Both counting methods showed a significantly decreased CNF count among the rapid progressors than among the slow progressors; the decline was more robust by using the automated detection algorithm ($P = 0.024$ for manual counts; $P = 0.0061$ for automated counts) (Figure 3, F and G). CNF loss was uniform across sample fields in individual animals. Neither manual nor automated CNF counts from uninfected control animals were significantly different from corneal nerve counts measured in slow progressors ($P > 0.05$). This was an expected finding, given that approximately 50% of persons infected with HIV do not have evidence of PNS damage.

Trigeminal Ganglia SIV Replication Levels

Previous studies have shown SIV replication in the sensory ganglia of dual-inoculated SIV-infected macaques at terminal end points.[16,17] To investigate whether SIV replication in the trigeminal ganglia differed between progressor groups,

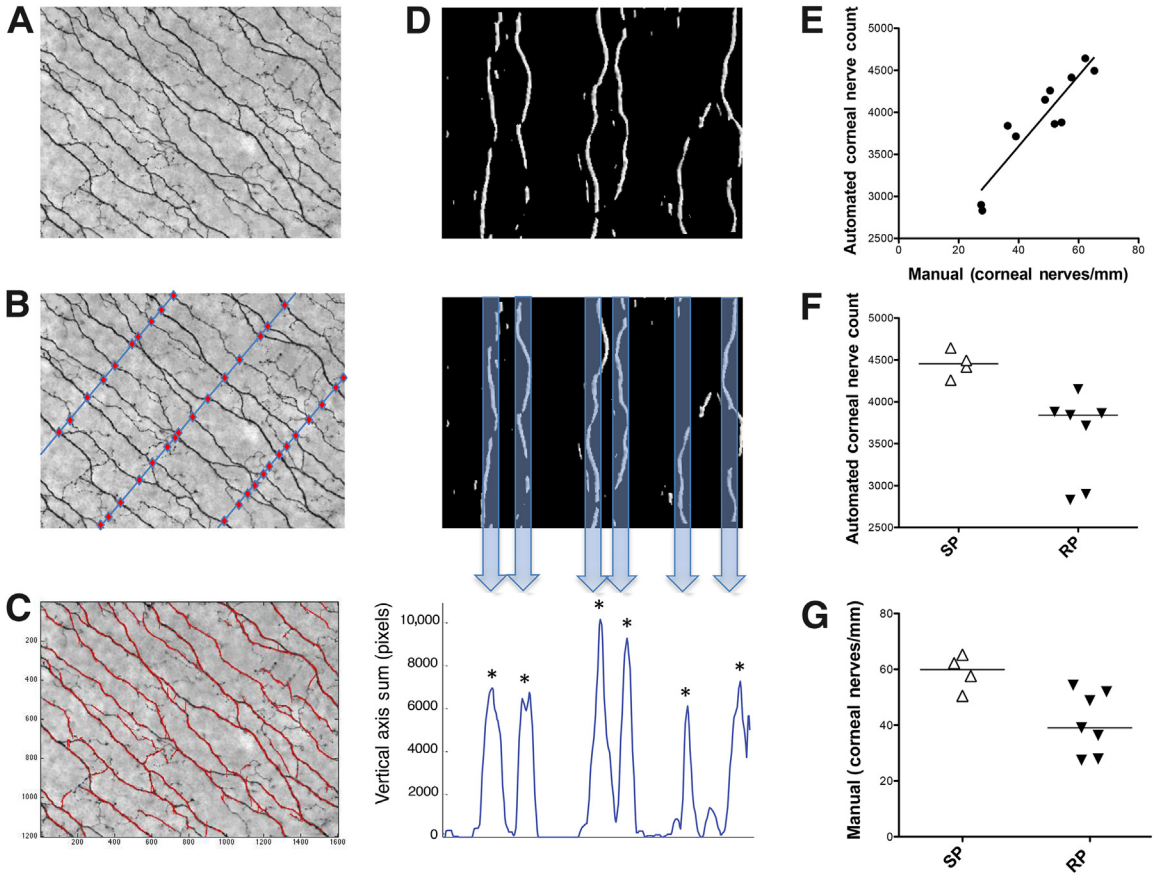

Figure 3 Manual and automated methods to measure CNF counts in RP compared with SP SIV-infected macaques. **A:** Image of the SBP of an RP animal represents the βIII tubulin immunostained images acquired for both the manual and automated quantitative assessment of CNF. **B:** For manual quantitative assessment, transects (**blue lines**) were drawn perpendicular to the longitudinal nerve trunks and nerve fibers crossing each transect (denoted by **red circles**) were counted. The number of nerve fibers counted was then divided by the length of each transect, and the average number of nerves per millimeter was calculated. **C:** The automated method used a custom algorithm (Voxeleron) to identify and then quantify CNFs. Applying filters generated an output image that depicted which nerve fibers would be detected by the algorithm. **D:** The automated algorithm used a series of steps to count nerve fibers. Each ×200 image was first subdivided into 16 smaller images that were then rotated to achieve a vertical orientation (**top panel**). The image pixel data were then summed along the vertical axis (**middle panel**), generating a 1D profile in which each peak represented a single nerve fiber denoted by an **asterisk** at the top of counted nerve fibers (**bottom panel**). Lower peaks that did not correspond to a nerve fiber were excluded by thresholding. **E:** A strong positive correlation was found between the two counting methods. **F:** A statistically significant decrease in CNFs among the RP group versus the SP group was found by using the automated method of quantitative assessment. **G:** Similarly, the manual method of quantitative assessment also found a statistically significant decrease in CNFs among the RPs. Lines represent median values (**E**–**G**). $P = 0.0061$ and $P = 0.024$ (**G**), both by Mann-Whitney test; and $P = 0.0004$, $r = 0.90$, Spearman rank correlation (**G**). Original magnification ×200 (**A**–**C**). RP, rapid progressors; SP, slow progressors.

SIV RNA levels were measured by quantitative RT-PCR. SIV RNA in the trigeminal ganglia among the rapid progressors was significantly elevated (median SIV RNA = 1076 copies/μg RNA; $P = 0.024$) (Figure 1B) compared with the slow progressors with low to undetectable SIV RNA levels (median SIV RNA = 3 copies/μg RNA).

Cellular Immune Responses in Trigeminal Ganglia

In the sensory ganglia of macaques, key cellular immune responders, including macrophages and satellite cells, are activated in response to SIV infection.[16,17] To determine whether there were differences in cellular immune responses between the rapid progressor and slow progressor groups, trigeminal ganglia sections were stained separately for the macrophage marker CD68 and the satellite cell marker GFAP. The amount of CD68 and GFAP immunostaining was then measured by quantitative image analysis.[29] Immunostaining for both CD68-positive macrophages and GFAP-expressing satellite cells was higher in the rapid progressor group than in the slow progressor group ($P = 0.054$ and $P = 0.0095$, respectively) (Figure 1, C and D). Furthermore, both macrophage (CD68 immunostaining: $P = 0.014$, $r = 0.80$) and satellite cell activation (GFAP immunostaining: $P = 0.0031$, $r = 0.88$) were strongly correlated with SIV RNA levels in the trigeminal ganglia, thus indicating a positive relationship between the extent of productive SIV infection and corresponding severity of inflammation in the sensory ganglia.

The CNF count measured by the automated algorithm was inversely correlated with terminal PVL ($P = 0.040$, $r = -0.64$), indicating a relationship between the extent of productive SIV infection and corneal nerve damage. CNF density was also related to both the extent of SIV replication ($P = 0.067$, $r = -0.65$) and macrophage activation in the trigeminal ganglia ($P = 0.067$, $r = -0.61$), but the small group sizes in the study did not allow us to uncover definitive relationships. In contrast, satellite cell activation in the trigeminal ganglia was not associated with CNF count ($P = 0.10$, $r = -0.55$).

CNF Density versus ENF Measurements

To compare both manual and automated CNF counts with ENF densities, we measured ENF densities in plantar foot punches obtained from SIV-inoculated macaques immunostained for the nerve fiber marker PGP9.5. We previously have demonstrated that SIV induces loss of ENF in macaques.[17] Both manual and automated CNF counts were strongly correlated with ENF measurements ($P = 0.048$, $r = 0.62$ for manual counts; $P = 0.040$, $r = 0.064$ for automated counts) (Figure 4, A and B).

Discussion

Because the cornea is the most densely innervated tissue in the body, corneal nerve assessment is extremely sensitive for detecting damage to small sensory nerve fibers compared with other tests, including measurement of intraepidermal nerve fibers in the skin.[11,30] The potential for early detection of nerve damage, taken with the rapidity and noninvasiveness of *in vivo* CCM, has led to increased use of corneal nerve assessments to monitor and evaluate a variety of peripheral neuropathies, particularly diabetic PN.[12,14,31–33] Despite the high prevalence of HIV-PN, as well as the clinical similarities between HIV-PN and diabetic PN, alterations in corneal nerves among persons infected with HIV have not yet been explored. With the use of an SIV/macaque model that closely resembles HIV infection, this study indicated loss of CNFs in the corneal subbasal nerve plexus. Furthermore, CNF counts corresponded closely with measurements of ENF length. CNF loss also was associated with viral replication and cellular immune activation in the trigeminal ganglia, the location of the neuronal cell bodies of the corneal sensory nerve fibers. The relationship between inflammation and SIV replication in the trigeminal ganglia and CNF loss imply that damage to neurons in the trigeminal ganglia impairs the ability of neurons to maintain sensory nerve fiber integrity. Together, these findings indicate that emerging noninvasive techniques to measure CNF alterations such as *in vivo* CCM may be useful clinical tools to screen for and monitor progression of PN in patients infected with HIV.

Common critiques of current corneal nerve assessments include the requirement for time-intensive manual image analysis and confounding interobserver variability in the recognition of nerve fibers, underscoring the need for trained observers.[34,35] To overcome these difficulties, we developed a consistent cornea immunostaining and image acquisition protocol. To measure CNFs in the SBP, we then developed and validated two rapid, easily applied methods for nerve measurements in the SBP: a manual method that counts all nerve fibers crossing a given transect and an automated method that uses a custom algorithm to identify

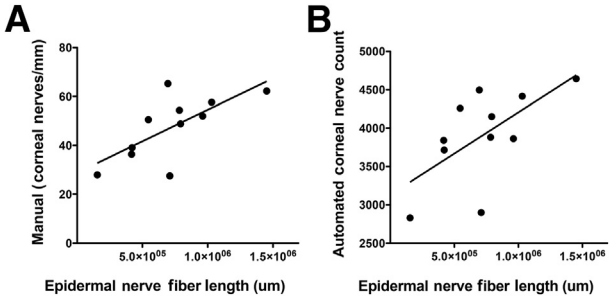

Figure 4 Relationship between ENF length and CNF counts obtained by using either manual or automated corneal counting methods. **A:** A significant, direct correlation is observed between ENF length and CNF density by using the manual method of quantitative assessment. **B:** The automated method of CNF quantitative assessment also shows a significant, direct correlation between CNF and ENF length, indicating the potential of CNF assessment as a surrogate measure in the evaluation of HIV-PN. Lines represent median values. $P = 0.048$, $r = 0.62$ (**A**) and $P = 0.040$, $r = 0.64$ (**B**), both Spearman rank correlation.

and count nerve fibers. Although both methods offer viable methods of assessment, the benefit of an automated method includes elimination of interobserver variability, thereby eliminating counting bias and subjectivity.

Both counting methods showed decreased CNF density in the rapid progressor group; the difference between the rapid and slow progressor groups was most pronounced with the use of the automated method of nerve detection. This discrepancy may reflect our method of immunostaining that enhances visibility of all CNFs as well as the differences in the sensitivity of nerve fiber detection between the methods. With the use of the manual method, every nerve fiber is counted regardless of size or thickness to reduce counting subjectivity. In contrast, the automated algorithm is less likely to identify very fine nerve branches, with detection largely limited to the thicker nerve trunks, similar to current *in vivo* CCM technology wherein many of the very fine nerve fibers also elude detection.[15,36] The difference in nerve fiber populations identified suggests that the density of thicker nerve trunks may better reflect the severity of CNF damage in SIV.

In this study, to reduce analysis time and to minimize observer variability, we focused on CNF density measurements, a parameter shown to have high intraobserver and interobserver repeatability and agreement.[37] However, other morphological parameters such as fiber length, branch density, and tortuosity of subbasal corneal nerves also have been shown to undergo significant changes throughout progression of PN disease, even when clinical symptoms are mild or absent and skin ENF measurements appear normal.[12–15,30,38] Future studies that use corneal nerve assessment as a surrogate for HIV-PN should also include measurements of these parameters to expand our understanding of CNF damage as well as repair throughout the course of infection. Moreover, in this study we were limited to terminal end points of disease because of the immunohistochemical staining method of nerve visualization that necessitated dissected corneal whole mounts. However, the move to noninvasive and thus repeatable methods of nerve detection such as *in vivo* CCM would enhance study of PN by enabling early detection of damage and progression of nerve fiber deterioration and would enable assessment of therapeutic strategies in the SIV/macaque model. Furthermore, adapting *in vivo* CCM for use in tracking HIV-induced PNS damage in patients may be of great value in identifying and preventing early PNS damage independent of performing skin biopsies.

Acknowledgments

We thank Rachel Weinberg, Dr. Ming Li, Bruce Baldwin, and Dr. Gigi Ebenezer for excellent technical support.

References

1. McArthur JC, Brew BJ, Nath A: Neurological complications of HIV infection. Lancet Neurol 2005, 4:543–555
2. Ellis RJ, Rosario D, Clifford DB, McArthur JC, Simpson D, Alexander T, Gelman BB, Vaida F, Collier A, Marra CM, Ances B, Atkinson JH, Dworkin RH, Morgello S, Grant I; CHARTER Study Group: Continued high prevalence and adverse clinical impact of human immunodeficiency virus-associated sensory neuropathy in the era of combination antiretroviral therapy: the CHARTER Study. Arch Neurol 2010, 67:552–558
3. Cornblath DR, McArthur JC: Predominantly sensory neuropathy in patients with AIDS and AIDS-related complex. Neurology 1988, 38: 794–796
4. Pardo CA, McArthur JC, Griffin JW: HIV neuropathy: insights in the pathology of HIV peripheral nerve disease. J Peripher Nerv Syst 2001, 6:21–27
5. Polydefkis M, Yiannoutsos CT, Cohen BA, Hollander H, Schifitto G, Clifford DB, Simpson DM, Katzenstein D, Shriver S, Hauer P, Brown A, Haidich AB, Moo L, McArthur JC: Reduced intraepidermal nerve fiber density in HIV-associated sensory neuropathy. Neurology 2002, 58:115–119
6. Sumner CJ, Sheth S, Griffin JW, Cornblath DR, Polydefkis M: The spectrum of neuropathy in diabetes and impaired glucose tolerance. Neurology 2003, 60:108–111
7. Smith AG, Howard JR, Kroll R, Ramachandran P, Hauer P, Singleton JR, McArthur J: The reliability of skin biopsy with measurement of intraepidermal nerve fiber density. J Neurol Sci 2005, 228: 65–69
8. Gonzalez-Duarte A, Cikurel K, Simpson DM: Managing HIV peripheral neuropathy. Curr HIV/AIDS Rep 2007, 4:114–118
9. Gonzalez-Duarte A, Robinson-Papp J, Simpson DM: Diagnosis and management of HIV-associated neuropathy. Neurol Clin 2008, 26: 821–832. x
10. Boulton AJ: Management of Diabetic Peripheral Neuropathy. Clin Diabetes 2005, 23:9–15
11. Müller LJ, Marfurt CF, Kruse F, Tervo TM: Corneal nerves: structure, contents and function. Exp Eye Res 2003, 76:521–542
12. Malik RA, Kallinikos P, Abbott CA, van Schie CH, Morgan P, Efron N, Boulton AJ: Corneal confocal microscopy: a non-invasive surrogate of nerve fibre damage and repair in diabetic patients. Diabetologia 2003, 46:683–688
13. Kallinikos P, Berhanu M, O'Donnell C, Boulton AJ, Efron N, Malik RA: Corneal nerve tortuosity in diabetic patients with neuropathy. Invest Ophthalmol Vis Sci 2004, 45:418–422
14. Midena E, Brugin E, Ghirlando A, Sommavilla M, Avogaro A: Corneal diabetic neuropathy: a confocal microscopy study. J Refract Surg 2006, 22:S1047–S1052
15. He J, Bazan HEP: Mapping the nerve architecture of diabetic human corneas. Ophthalmology 2012, 119:956–964
16. Laast VA, Pardo CA, Tarwater PM, Queen SE, Reinhart TA, Ghosh M, Adams RJ, Zink MC, Mankowski JL: Pathogenesis of simian immunodeficiency virus-induced alterations in macaque trigeminal ganglia. J Neuropathol Exp Neurol 2007, 66:26–34
17. Laast VA, Shim B, Johanek LM, Dorsey JL, Hauer PE, Tarwater PM, Adams RJ, Pardo CA, McArthur JC, Ringkamp M, Mankowski JL: Macrophage-mediated dorsal root ganglion damage precedes altered nerve conduction in SIV-infected macaques. Am J Pathol 2011, 179: 2337–2345
18. Marfurt CF, Cox J, Deek S, Dvorscak L: Anatomy of the human corneal innervation. Exp Eye Res 2010, 90:478–492
19. Clements JE, Mankowski JL, Gama L, Zink MC: The accelerated simian immunodeficiency virus macaque model of human immunodeficiency virus-associated neurological disease: from mechanism to treatment. J Neurovirol 2008, 14:309–317
20. Kelly KM, Tarwater PM, Karper JM, Bedja D, Queen SE, Tunin RS, Adams RJ, Kass DA, Mankowski JL: Diastolic dysfunction is associated with myocardial viral load in simian immunodeficiency virus-infected macaques. AIDS 2012, 26:815–823
21. Perona P, Malik J: Scale-space and edge-detection using anisotropic diffusion. IEEE Trans Pattern Anal Mach Intell 1990, 12:629–639

22. Frangi AF, Niessen WJ, Vincken KL, Viergever MA: Multiscale vessel enhancement filtering. Lect Notes Comput Sc 1998, 1496:130–137
23. Holland NR, Stocks A, Hauer P, Cornblath DR, Griffin JW, McArthur JC: Intraepidermal nerve fiber density in patients with painful sensory neuropathy. Neurology 1997, 48:708–711
24. McCarthy BG, Hsieh ST, Stocks A, Hauer P, Macko C, Cornblath DR, Griffin JW, McArthur JC: Cutaneous innervation in sensory neuropathies: evaluation by skin biopsy. Neurology 1995, 45:1848–1855
25. Nolano M, Provitera V, Crisci C, Stancanelli A, Wendelschafer-Crabb G, Kennedy WR, Santoro L: Quantification of myelinated endings and mechanoreceptors in human digital skin. Ann Neurol 2003, 54:197–205
26. Ebenezer GJ, McArthur JC, Polydefkis M, Dorsey JL, O'Donnell R, Hauer P, Adams RJ, Mankowski JL: SIV-induced impairment of neurovascular repair: a potential role for VEGF. J Neurovirol 2012, 18: 222–230
27. Ebenezer GJ, O'Donnell R, Hauer P, Cimino NP, McArthur JC, Polydefkis M: Impaired neurovascular repair in subjects with diabetes following experimental intracutaneous axotomy. Brain 2011, 134: 1853–1863
28. Mouton PR, Gokhale AM, Ward NL, West MJ: Stereological length estimation using spherical probes. J Microsc 2002, 206:54–64
29. Mankowski JL, Queen SE, Tarwater PM, Fox KJ, Perry VH: Accumulation of beta-amyloid precursor protein in axons correlates with CNS expression of SIV gp41. J Neuropathol Exp Neurol 2002, 61:85–90
30. Quattrini C, Tavakoli M, Jeziorska M, Kallinikos P, Tesfaye S, Finnigan J, Marshall A, Boulton AJ, Efron N, Malik RA: Surrogate markers of small fiber damage in human diabetic neuropathy. Diabetes 2007, 56:2148–2154
31. Tavakoli M, Marshall A, Pitceathly R, Fadavi H, Gow D, Roberts ME, Efron N, Boulton AJ, Malik RA: Corneal confocal microscopy: a novel means to detect nerve fibre damage in idiopathic small fibre neuropathy. Exp Neurol 2010, 223:245–250
32. Tavakoli M, Marshall A, Thompson L, Kenny M, Waldek S, Efron N, Malik RA: Corneal confocal microscopy: a novel noninvasive means to diagnose neuropathy in patients with Fabry disease. Muscle Nerve 2009, 40:976–984
33. Tavakoli M, Quattrini C, Abbott C, Kallinikos P, Marshall A, Finnigan J, Morgan P, Efron N, Boulton AJM, Malik RA: Corneal confocal microscopy: A novel noninvasive test to diagnose and stratify the severity of human diabetic neuropathy. Diabetes Care 2010, 33: 1792–1797
34. Turuwhenua JT, Patel DV, McGhee CN: Fully automated montaging of laser scanning in vivo confocal microscopy images of the human corneal subbasal nerve plexus. Invest Ophthalmol Vis Sci 2012, 53: 2235–2242
35. Patel DV, McGhee CN: Quantitative analysis of in vivo confocal microscopy images: a review. Surv Ophthalmol 2013, 58:466–475
36. Tavakoli M, Hossain P, Malik RA: Clinical applications of corneal confocal microscopy. Clin Ophthalmol 2008, 2:435–445
37. Petropoulos IN, Manzoor T, Morgan P, Fadavi H, Asghar O, Alam U, Ponirakis G, Dabbah MA, Chen X, Graham J, Tavakoli M, Malik RA: Repeatability of in vivo corneal confocal microscopy to quantify corneal nerve morphology. Cornea 2013, 32:e83–e89
38. Edwards K, Pritchard N, Vagenas D, Russell A, Malik RA, Efron N: Utility of corneal confocal microscopy for assessing mild diabetic neuropathy: baseline findings of the LANDMark study. Clin Exp Optom 2012, 95:348–354